Somatostatin-positive neurons in the reticular thalamus modulate gamma rhythms and visual information in mouse V1

Mahmood S. Hoseini[1#], Bryan Higashikubo[2#], Frances S. Cho[2,3,4,5], Andrew H. Chang[2], Alexandra Clemente-Perez,[2,3,5], Irene Lew[2], Michael Stryker[1,3,5], Jeanne T. Paz[2,3,4,5*]

[1] University of California, San Francisco, Department of Physiology, CA, 94158, USA; [2] Gladstone Institute of Neurological Disease, San Francisco, CA, 94158 USA; [3] University of California, San Francisco, Neurosciences Graduate Program, CA, 94158 USA; [4] University of California, San Francisco, Department of Neurology, CA, 94158 USA; [5] Kavli Institute for Fundamental Neuroscience, University of California San Francisco

ABSTRACT

Visual perception in natural environments depends on the ability to focus on salient stimuli while ignoring distractions. This kind of selective visual attention is associated with gamma oscillations in the visual cortex. While the nucleus reticularis thalami (nRT) has been implicated in selective attention, its role in modulating visual perception remains unknown. Here we show that somatostatin-expressing neurons (SOM) in the nRT preferentially project to visual thalamic nuclei, as compared to the more abundant parvalbumin-expressing neurons, and powerfully modulate both visual information transmission and gamma oscillations in the primary visual cortex (V1). These findings represent a novel circuit through which the nRT can influence representation of visual information.

KEYWORDS: Reticular thalamic nucleus, Gamma oscillations, Thalamocortical visual circuits, Visual cortex, Information transmission, Optogenetics

INTRODUCTION

Visual perception relies on the ability to focus on important information while ignoring distractions. Such selective attention is associated with neural oscillations in the gamma frequency band (~30-90 Hz, "gamma oscillations") in the visual cortices in both rodents and humans (Engel et al., 2001; Taylor et al., 2005; Pavlova et al., 2006; Doesburg et al., 2008; Ray et al., 2008b; Siegel et al., 2008). Gamma oscillations, particularly in the visual cortex, are associated with a high level of cortical activity, and some have speculated that they may play a causal role in perception and the focusing of attention (Gray et al., 1992; Singer and Gray, 1995; Kreiter and Singer, 1996) or in enabling a time-division multiplexing of cortical responses to multiple simultaneous stimuli (Stryker, 1989). Electro-corticographic (ECoG) studies have shown a clear correlation between focal increases in high gamma and cortical responses to stimulation measured by other means (Ray et al., 2008a; Yazdan-Shahmorad et al., 2013). Whether gamma oscillations play a causal role in brain function or merely represent the "ringing" of an insufficiently damped response of the cortical circuit to a strong input is not clear. However, studies have shown that the effective output of primary sensory cortical areas to peripheral stimulation is much greater during a particular phase of gamma, and that increasing gamma and synchronized cortical activity by optogenetic stimulation at the appropriate phase with respect to a sensory stimulus can change the number of spikes elicited (Cardin et al., 2009; Sohal et al., 2009).

Moreover, two types of gamma oscillations have been reported in the primary visual cortex (V1) differentiated by whether they result from intra-cortical or subcortical inputs

*Correspondence to: jeanne.paz@gladstone.ucsf.edu
* Lead Contact: Jeanne T. Paz, PhD
#Authors equally contributed to work
Number of Text Pages in this main document: 25
Number of main Figures: 6
Number of main Tables: 1
Supplementary Material: 3 Figures, legends, 0 Videos, 0 Tables

through the dorsal lateral geniculate nucleus (dLGN) (Saleem et al., 2017). All visual input to the cortex has to pass through the thalamus, which gates the flow of visual information to the cortex. The GABAergic nucleus reticularis thalami (nRT) (Houser et al., 1980) provides a powerful source of GABAergic inhibition for thalamocortical neurons (Sherman and Koch, 1986; McCormick and Bal, 1997; Gentet and Ulrich, 2003; Lam and Sherman, 2011; Halassa and Acsády, 2016; Crabtree, 2018), allowing the nRT to control different information streams to the cortex. The nRT has been regarded as "the guardian of the gateway" to the cortex (Crick, 1984; McAlonan et al., 2008; Halassa and Acsády, 2016), and is well positioned to exert attentional selection by controlling which thalamocortical "channel" of information the cortex should "pay attention to". Optogenetic activation of inhibitory (Gad2-positive) neurons in the dorsal portion of the nRT transiently reduces activity in the dorsal lateral geniculate nucleus (dLGN), the source of the specific sensory input to V1, particularly in its input layer (Lien and Scanziani, 2013). However, it is unknown whether inputs other than the strength of peripheral stimulation control the magnitude of gamma oscillations in V1. Here, we investigated whether nRT modulates gamma oscillations and the representation of visual information in V1 in behaving mice both during locomotion and while standing still, and with and without visual stimulation.

RESULTS

Visual thalamocortical nuclei receive projections from SOM nRT neurons

To determine whether the visual thalamocortical relay nuclei receive inputs from somatostatin- (SOM) and/or parvalbumin- (PV) expressing neurons of the nRT, we injected an AAV viral construct encoding enhanced yellow fluorescent protein (eYFP) in the nRT of SOM-Cre and PV-Cre mice (**Figure 1**). We previously validated this approach immunohistochemically and showed that SOM and PV neurons of the nRT target distinct midline and somatosensory thalamocortical relay nuclei, respectively (Clemente-Perez et al., 2017). In the nRT, SOM and PV cell bodies and their axons robustly expressed eYFP four weeks post-injection. Confocal microscopy revealed dense axonal boutons from SOM nRT neurons in the dLGN, but only very sparse input from PV nRT neurons (**Figure 1**). This was surprising given that PV neurons represent the major cellular population of nRT (Clemente-Perez et al., 2017). As previously shown, PV but not SOM neurons from the nRT projected densely to the somatosensory ventroposteromedial (VPM) thalamocortical nucleus (**Figure 1**).

We validated that the virus specifically targeted the nRT by serially sectioning the brain and noting the eYFP somatic expression in all mice as described in our previous study (Clemente-Perez et al., 2017). Immunohistochemistry confirmed that SOM and PV populations in nRT were distinct, as described previously (Clemente-Perez et al., 2017).

Optogenetic activation of SOM nRT neurons reduces single-cell responses and gamma power in V1 both with and without visual stimulation

To determine whether disrupting activity of SOM nRT neurons affects visual responses in V1, we injected an AAV viral construct containing channelrhodopsin (ChR2) in the nRT of SOM-Cre mice. Thereafter, extracellular recordings of single unit activity and local field potentials (LFPs) were made using a double-shank 128-channel microelectrode array placed in the V1 of mice that were free to stand or run on a polystyrene ball floating on an air stream (**Figure 2A**) (Du et al., 2011; Hoseini et al., 2019). Mice viewed a gray blank screen while a blue light (473 nm, ~63 mW/mm^2) was delivered using an optical fiber implanted above nRT. Optogenetic activation of SOM cells in nRT greatly reduced the power of LFPs across almost all frequencies regardless of the locomotion state of the animal (**Figure 2B**). Optogenetic activation significantly reduced across-trial average power (scaled by 1/f) in all recording channels and all frequencies, especially in the gamma band (**Figure 2C**, **Table 1**). Consistent with previous findings, locomotion differently modulated power across different frequencies (**Figure 2D**) (Niell and Stryker, 2010). Locomotion caused a moderate power increase at low frequencies (<10 Hz), a moderate decrease in the beta band (15-30 Hz), and a dramatic power increase at higher frequencies in the gamma band (30-80 Hz) (**Fig-**

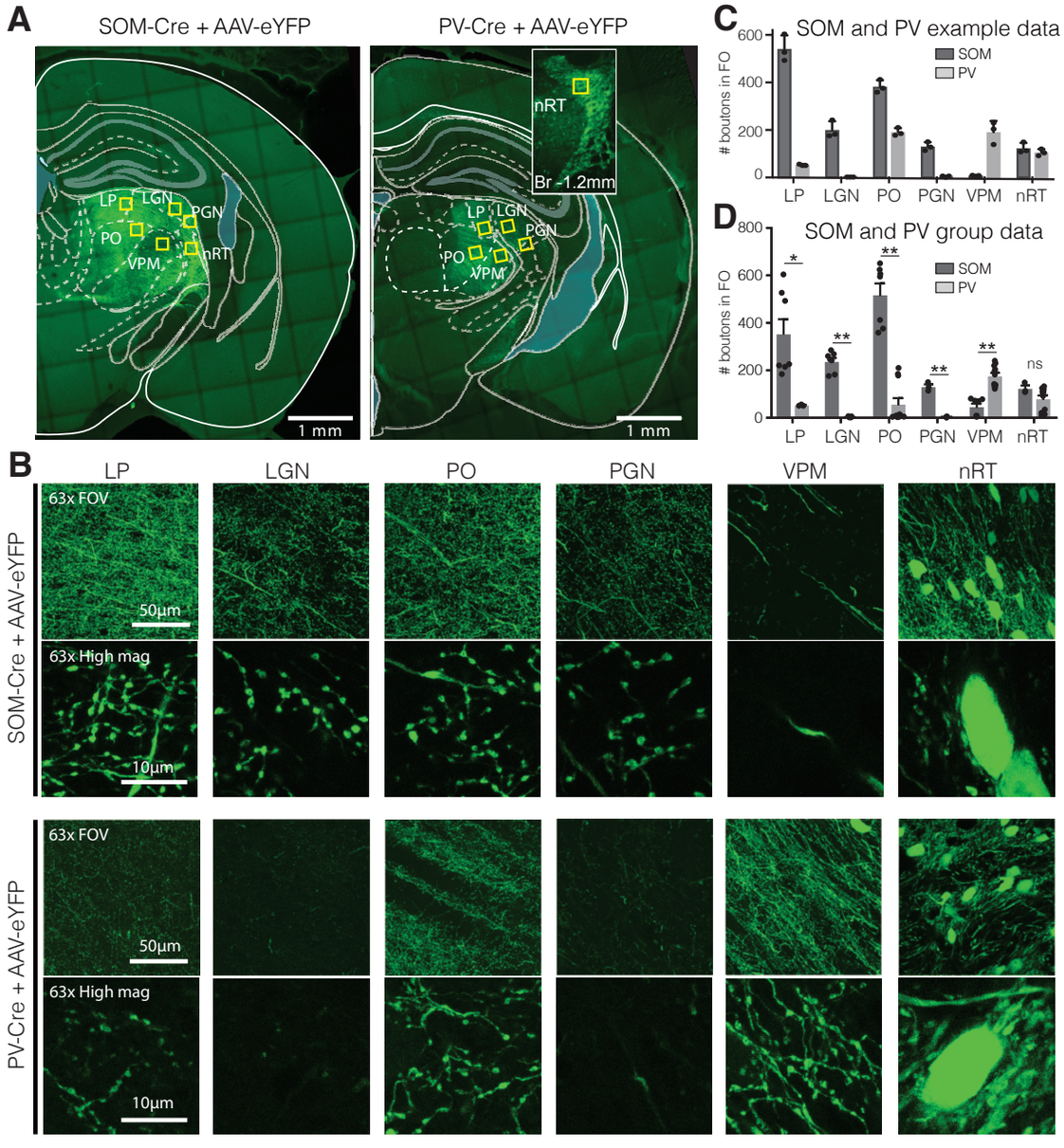

Figure 1. Visual relay thalamic nuclei are preferentially targeted by SOM and not PV GABAergic neurons from nRT. A, Representative example sections of SOM-Cre and PV-Cre mice after injection of floxed AAV in nRT. Yellow boxes indicate locations chosen for 63x confocal imaging and putative bouton quantification. Inset: nRT injection site as seen in an adjacent section. **B,** 63x confocal images showing the entire field of view (FOV) and a zoomed cropped region ('High mag') to show details of axonal boutons and nRT somata. LP: lateral posterior nucleus; LGN: dorsal lateral geniculate nucleus; PO: posterior medial nucleus; PGN: pregeniculate nucleus (also referred to as ventral LGN); VPM: ventroposteromedial nucleus; nRT: thalamic reticular nucleus. The expression of the viral constructs in different brain regions was confirmed using the mouse brain atlas (Paxinos and Franklin, 2001). **C,** Number of eYFP-labeled boutons present in thalamic nuclei of representative mice shown in panel A. Data taken from three consecutive sections from each mouse. **D,** Number of eYFP-labeled boutons present in thalamic nuclei of all mice imaged (n = 2 SOM-Cre, 3 PV-Cre, 3-4 sections per mouse). Differences are significant between genotypes for all regions except for nRT after correction for multiple comparisons. *p<0.05, **p<0.01.

ure 2D and **Table 1**). Averaging power across all channels showed that optogenetic activation of SOM neurons in nRT nearly abolished power across the three bands in the still condition (**Figure 2E**, **Table 1**). In contrast, during locomotion optogenetic activation strongly reduced gamma power (**Figure 2E**, **Table 1**).

To investigate how evoked visual responses are affected by optogenetic activation of SOM nRT cells, visual responses were recorded to drifting sinusoidal gratings presented in the visual field contralateral to the recording site, and SOM nRT neurons were activated optogenetically during randomly interleaved trials (**Figure 2F**). While visual stimulation selectively enhanced beta- and gamma-band LFP power, optogenetic activation increased theta power and markedly reduced power in the other two frequency bands (**Figure 2G-I—figure supplement 1, Table 1**). Firing rates of isolated neurons were also modulated by optogenetic activation of SOM nRT neurons. Neurons were classified as narrow- or broad-spiking using three parameters calculated from average spike waveforms (Niell and Stryker, 2008) (**Figure 2J**). Narrow-spiking cells consist of fast-spiking interneurons, whereas broad-spiking cells are 90% excitatory and 10% inhibitory cells (Barthó et al., 2004; Atencio and Schreiner, 2008). Hereafter, for clarity, we refer to the narrow-spiking units as inhibitory neurons (abbreviated as NS) and broad-spiking units as excitatory neurons (abbreviated as BS). Optogenetic activation of SOM nRT neurons significantly suppressed activity of both cell types during both stationary and locomotion states (**Figure 2K**, **Table 1**). Locomotion continued to increase the firing rates even in the presence of optogenetic activation (**Figure 2K**, **Table 1**). No clear relationship was observed between the changes in each neuron's firing rate and the LFP power at its recording site (**Figure 2L**).

As a control experiment, we tested for potential non-specific effects of the laser light used for optogenetic activation by making recordings in the cortex of SOM-Cre mice that were injected with an AAV viral construct containing eYFP in the nRT. Visual responses were recorded with and without optogenetic light during interleaved trials (**Figure 3A, D**). As expected, delivering the optogenetic stimulus light (blue, 473 nm, ~63 mW/mm^2) had no effect on the power across different frequency bands with (**Figure 3E**, **Table 1**) or without (**Figure 3B**, **Table 1**) visual stimulation; nor did it alter the firing rates of individual neurons (**Figure 3F**, **Table 1**). The effects of locomotion were not altered by the laser (**Figure 3C**, **Table 1**).

To test whether different cortical layers are disproportionately modulated by the optogenetic activation of SOM nRT cells, we compared the changes in visual responses at individual recording sites. While visual stimuli evoked the strongest responses in the superficial layers (~layer 2/3) and layer 4 (**Figure 4A—figure supplement 2**), optogenetic activation of SOM nRT neurons reduced activity most strongly in layer 2/3 (**Figure 4B**). Excluding the most superficial recording sites, where effects were variable, the greatest difference between evoked spike responses in the presence and absence of optogenetic activation of SOM nRT cells was between 200 and 600 μm from the cortical surface in every case (**Figure 4C, D**).

Optogenetic inhibition of SOM nRT neurons enhances gamma power in V1 with and without visual stimulation

An alternative approach to determine how nRT gates visual information is to inhibit SOM nRT neurons. The outcome of this experiment is not trivial since optogenetic activation and inactivation of neurons do not necessarily produce symmetric effects (Phillips and Hasenstaub, 2016; Moore et al., 2018). For this purpose, we injected an AAV viral construct containing Halorhodopsin (eNpHR) into the nRT of SOM-Cre mice, and then recorded neural activity as in the ChR2 experiments following optical stimulation with a green light (532 nm, ~104 mW/mm^2) (**Figure 5A**). Optogenetic inhibition of SOM cells in nRT enhanced LFP power across a wide range of frequencies regardless of the locomotion state of the animal (**Figure 5B**). Across-trial average power (scaled by 1/f) was significantly reduced in the theta band and increased in the beta and gamma bands across all channels (**Figure 5C, E, Table 1**) in the absence of visual stimulation (**Figure 5D, Table 1**). Inhibition of SOM nRT neurons during visual stimulation similarly produced a great increase in gamma-band LFP power but reduced power at frequencies below 30 Hz (**Figure 5F-I, Table 1**). Finally, optogenetic inhibition of SOM nRT neurons increased the firing rates of

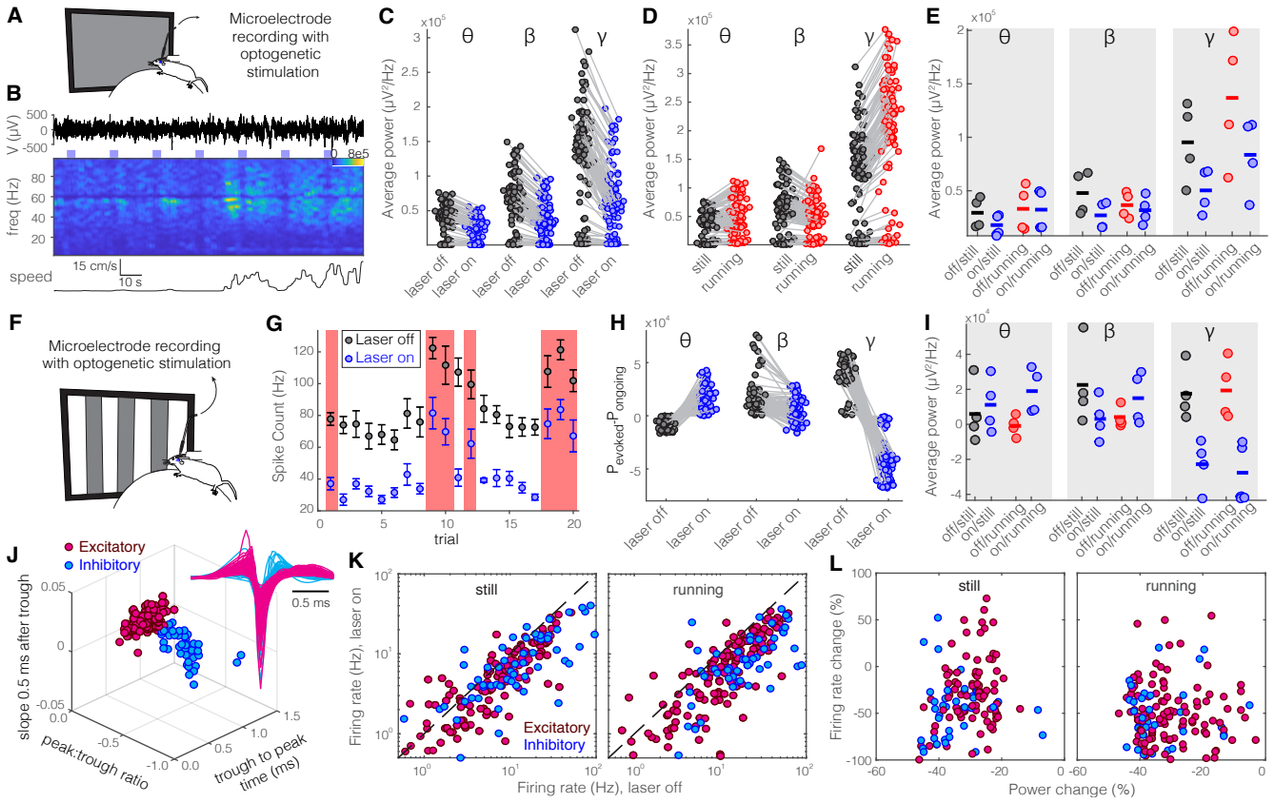

Figure 2. Optogenetic activation of SOM nRT neurons reduces gamma activity in V1 both with and without visual stimulation. A, Neural activity was recorded from the primary visual cortex of freely-moving mice. Mice were presented with a gray blank screen while a blue light (473 nm, ~63 mW/mm2) was delivered to ChR2-expressing SOM cells in nRT using an optical fiber implanted above the nRT. Mouse movement was tracked over the course of the experiment. **B,** Representative extracellular raw voltage trace is shown along with its power spectrum. Blue shading areas indicate optogenetic activation. Mouse movement speed is shown at the bottom. **C,** Across-trial average power of all channels in the absence (black) and presence (blue) of optogenetic activation in one representative mouse shows a moderate decrease across theta (4-8 Hz) and beta (15-30 Hz) bands and a strong decrease in gamma band (30-80 Hz) (See Table 1 for statistics). **D,** Across-trial average power of all channels in one representative mouse indicates that locomotion slightly modulates theta and beta powers, while causing a strong enhancement in gamma power (Table 1). **E,** Average power across all channels shows that optogenetic activation of SOM nRT cells greatly reduces power across the three bands in the still condition (black vs. blue marks). Optogenetic activation of SOM nRT cells strongly modulates gamma power when the mice are running (red vs. blue marks). **F,** Visual responses were recorded while mice were presented with moving gratings (8 directions, each moving in one of two possible directions; 2 s duration; randomly interleaved with optogenetic stimulation) in the visual field contralateral to the recording site. **G,** Firing rate (averaged over all 12 drifting directions) of an example cell during the course of experiment. Black marks: visual responses when the laser is off; Blue marks: visual responses when visual stimuli and optogenetic activation of SOM nRT cells are coupled. Red shadings: locomotion state. Error bars: SEM. **H,** Evoked power (average over all 20 trials) of all channels when the laser is off (black circles) versus the laser-on condition (blue circles) indicates a significant shift across all frequencies (Table 1). **I,** Same as in Fig. 2E for still and running conditions (Table 1). **J,** Using the three parameters calculated from average waveforms, cells were classified into narrow- (inhibitory, cyan) or broad- (excitatory, magenta) spiking (height of the positive peak relative to the negative trough: -0.20 ± 0.01, -0.34 ± 0.02 (p=1.02e-9, Wilcoxon rank-sum test) slope of the waveform 0.5 ms after the negative trough: 0.73 ± 0.02, 0.32 ± 0.02 (p=3.9e-33), the time from the negative trough to the peak: 0.01 ± 0.00, -0.01 ± 0.00 ms (p=5.94e-35), excitatory (n=169) and inhibitory (n=73) cells respectively). Subplot: average spike waveforms for all units, aligned to minimum, demonstrating excitatory (magenta) and inhibitory (cyan) cells. **K,** Firing rate of excitatory (magenta) and inhibitory (cyan) cells across different conditions (Table 1). **L,** Percentage change in firing rate of both cell type versus percentage change of power in channels that each cell is recorded on for still and running (Table 1, Spearsman's rho and p: 0.05, 0.58 BS & still; -0.12, 0.22 BS & running; 0.19, 0.29 NS & still; 0.05, 0.77 NS & running).

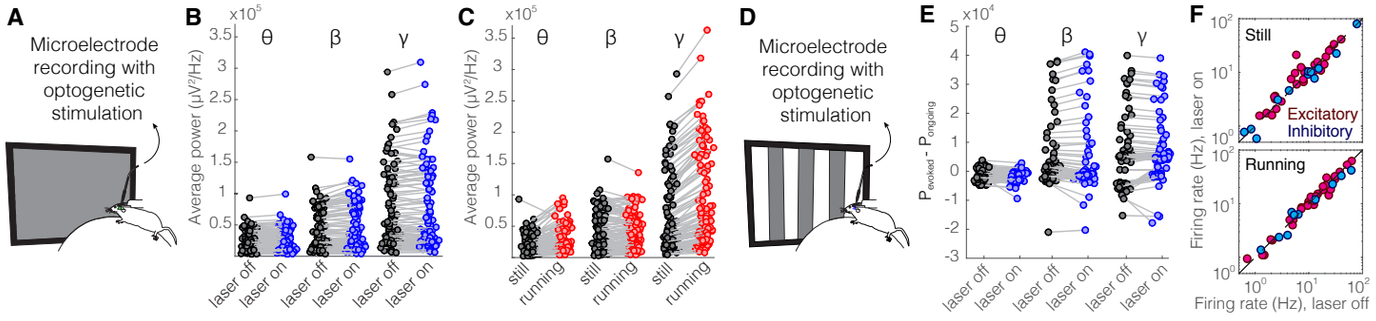

Figure 3. Optical stimulation of control eYFP-expressing SOM nRT neurons does not change V1 activity. A, Experimental setup. **B,** Across-trial average power of all 121 channels in the absence (black) and presence (blue) of optogenetic activation in one mouse shows no change (Table 1). **C,** Across-trial average power of all channels in one mouse indicates that locomotion slightly modulates theta and beta powers, while causing a strong enhancement in gamma power (Table 1). **D,** Visual responses were recorded while mice were presented with moving gratings. **E,** Average power across all channels shows that light delivery in eYFP-expressing SOM nRT cells does not affect power in V1 (Table 1). **F,** Firing rate of excitatory (magenta) and inhibitory (cyan) cells across different conditions are not affected by the light in mice in which nRT does not express the opsin (Table 1).

both excitatory and inhibitory cells in V1 (**Figure 5J-L, Table 1**). Overall, the effects of optogenetic inhibition of SOM nRT neurons were opposite to those of their activation but were somewhat smaller and less consistent.

Optogenetic activation of SOM nRT neurons diminishes encoding ability of excitatory and inhibitory cells in V1

The dense anatomical projection from SOM cells in nRT to visual thalamus raised the possibility that this class of cells gates the flow of visual information to V1. Since locomotion alters both strength and information content of visual responses (Niell and Stryker, 2008; Dadarlat and Stryker, 2017), we computed the mutual information conveyed by the spikes of single neurons about the visual stimuli with and without optogenetic activation of nRT SOM cells. Mutual information (I(R, S), see Materials and Methods) was computed separately for the running and stationary behavioral states. Optogenetic activation of SOM nRT neurons markedly reduced mutual information between the responses and our set of visual stimuli for both excitatory and inhibitory cells (**Figure 6A, D—figure supplement 3, Table 1**). The reduction of mutual information in individual V1 neurons during optogenetic inhibition of SOM cells in nRT suggests that activity of the V1 population as a whole would encode less information about visual stimuli. We estimated the representation of visual information in the response of the V1 population by training a linear decoder (LDA) to identify the visual stimulus that the animal was viewing in single stimulus trials on the basis of the spike responses in the entire population of recorded neurons. LDA incorporates the following three assumptions: that different visual stimuli evoke linearly separable responses, that evoked responses are independent across neurons, and that the responses have a Gaussian distribution. The decoder is trained on all data except a single trial which is left out for testing purposes (leave-one-out cross validation, LDA-LOOXV). This approach allows us to quantify how well parameters of the visual stimulus (orientation and direction) can be predicted for the single trials excluded from the training set.

Single-trial neuronal responses during locomotion were classified less accurately during optogenetic activation of SOM nRT cells for grating orientation in both excitatory (98% laser-off vs. 81% laser-on, p=2e-11, Wilcoxon rank-sum test) and inhibitory (86% vs. 58%, p=1e-13) cell types (**Figure 6B**, **E**). Importantly, this finding does not depend on the behavioral state of the animal (**Figure supplement 3C**). Moreover, repeating the decoding analysis separately including only cells that were in the same range of cortical depth (see **Figure 4D**) yielded similar accuracy, indicating no particular laminar distinction in stimulus encoding.

Optogenetic activation of SOM cells in nRT led to lower population spike counts on average, which in turn led to reduced

visual information (Figure supplement 3A). The observed reduction in visual information could therefore be due either to the reduction of neuronal firing rates or to changes in the pattern of neural responses. To distinguish between these two possibilities, we quantified decoding accuracy for trials with equal population spike counts (see Methods). We sampled (without replacement) anywhere between one and maximum number of neurons to get a very low or high number of spikes, respectively. This process was repeated 100 times and then decoding accuracy was compared for equal population spike counts during laser-off and laser-on states by including more cells in the laser-on than the laser-off classifier. LDA-LOOXV was performed separately for the data collected from each mouse and then the results from all four mice were pooled together to generate average decoding accuracy as a function of population spike count for each cell type, behavioral state, and optogenetic state. Not surprisingly, classification accuracy increased with increasing spike count across all conditions. However, accuracy was always lower during optogenetic activation of SOM nRT cells for equal population spike counts (**Figure 6C**, **F—Figure supplement 3**), and particularly so at high population spike counts. The difference was less prominent with optogenetic inhibition of SOM nRT neurons (**Figure supplement 3E-H**). These findings indicate that the activity of nRT SOM cells alters the pattern as well as the amount of neuronal activity in V1 that determines how accurately visual stimuli are encoded.

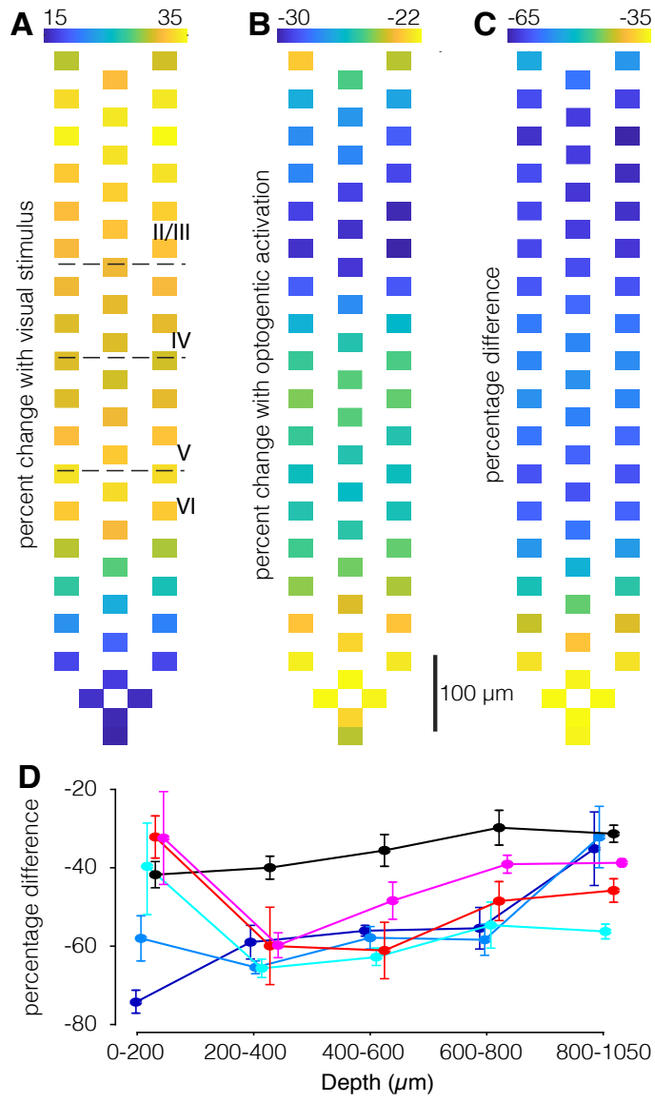

Figure 4. **Optogenetic activation of SOM nRT has a stronger effect on neuronal responses in superficial layers in V1 neuronal responses. A,** Percentage increase of average evoked visual responses relative to the average preceding ongoing activity overlaid over microelectrode map shows an increase of about 15 to 35%. **B,** Percentage change of average evoked visual activity in the presence of optogenetic light relative to the average preceding activity overlaid over microelectrode map. **C,** Percentage difference between evoked responses in the presence of laser light (panel B) and evoked responses in the absence of laser light (panel A). **D,** Percentage difference (panel C) quantified in bins of 200 microns across 6 shanks in recordings from 4 mice.

DISCUSSION

Here we identified a new subcortical circuit that modulates both gamma oscillations and the representation of information in the primary visual cortex. We found that the input from nRT to the dLGN in the mouse is from the class of inhibitory neurons that express somatostatin (SOM), with negligible anatomical connections from the more numerous parvalbumin-positive (PV) neurons. Optogenetic activation of SOM nRT neurons in alert, head-fixed mice suppressed both V1 spike and LFP responses to visual stimulation and caused a seconds-long suppression of gamma, whether the mice were stationary or running on a polystyrene ball floating on

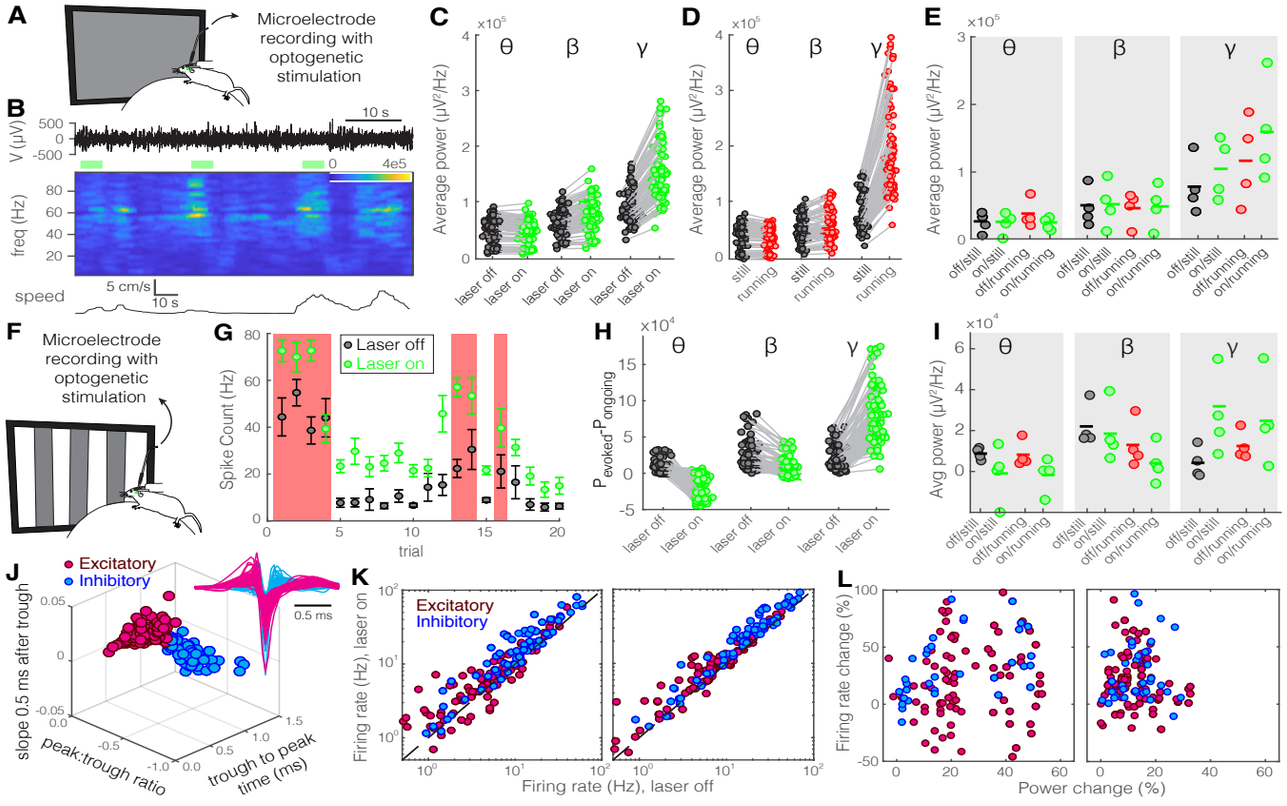

Figure 5. **Optogenetic inhibition of SOM nRT neurons enhances gamma activity in V1 both with and without visual stimulation. A,** Experimental setup. Mice were presented with a gray blank screen while a green light (532 nm, ~104 mW/mm2) was delivered to eNpHR-expressing SOM neurons in nRT. **B,** Representative extracellular raw voltage trace is shown along with its power spectrum recorded in V1. Green shading areas indicate optogenetic inhibition of the nRT. Mouse movement speed is shown at the bottom. **C,** Across-trial average power of all channels in the absence (black) and presence (green) of optogenetic inhibition of SOM nRT neurons in one representative mouse shows a moderate increase across theta and beta bands and a strong enhancement in gamma band (Table 1). **D,** Locomotion greatly enhances oscillation power in gamma band (Table 1). **E,** Average power across all 59 channels shows that optogenetic inhibition of SOM nRT neurons greatly increases gamma power during still (black vs. green marks) and running (red vs. green marks) (Table 1). **F,** Experimental setup. **G,** Firing rate (averaged over all 12 drifting directions) of an example cell during the course of experiment. Black marks: visual responses when the laser is off; Green marks: visual responses when visual stimuli and optogenetic inhibition of SOM nRT cells are coupled. Red shadings: locomotion state. Error bars: SEM. **H,** Across-trial average power of all channels in the absence (black) and presence (green) of optogenetic inhibition of SOM nRT in one mouse shows a decrease in theta and beta powers and a significant increase in gamma band (Table 1). **I,** Same as in Fig. 4E for still and running condition (Table 1). **J,** Using the three parameters calculated from average waveforms, cells were classified into narrow- (inhibitory, cyan) or broad- (excitatory, magenta) spiking (height of the positive peak relative to the negative trough: -0.19 ± 0.01, -0.28 ± 0.01 (p=3.2e-8, Wilcoxon rank-sum test) slope of the waveform 0.5 ms after the negative trough: 0.74 ± 0.01, 0.34 ± 0.01 (p=5.9e-30), the time from the negative trough to the peak: 0.01 ± 0.00, -0.01 ± 0.00 ms (p=1.2e-27), excitatory (n=97) and inhibitory (n=79) cells respectively). Shown in the subplot are the average spike waveforms for all units, aligned to minimum, demonstrating excitatory (magenta) and inhibitory (cyan) cells. **K,** Firing rate of excitatory (magenta) and inhibitory (cyan) cells across different conditions (Table 1). **L,** Percentage change in firing rate of both cell types versus percentage change of power in channels that each cell is recorded on for still and running (Table 1, Spearsman's rho, p_value: 0.14, 0.26 BS & still; -0.09, 0.44 BS & running; 0.61, 0.002 NS & still; 0.03, 0.89 NS & running).

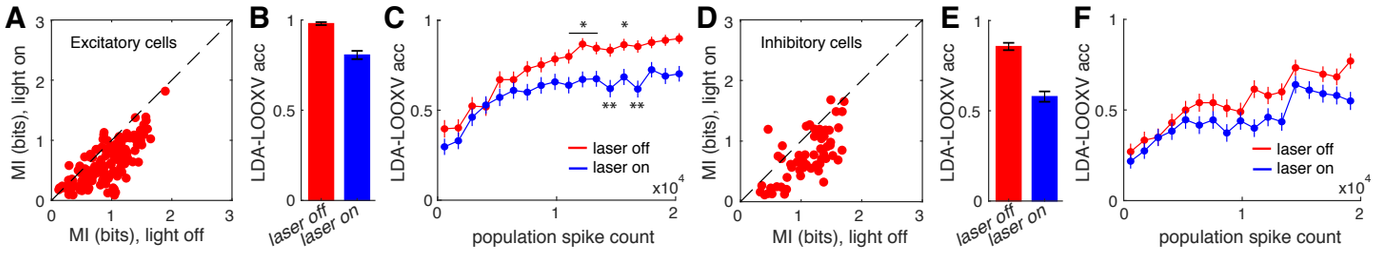

Figure 6. **Optogenetic activation of SOM nRT neurons diminishes encoding ability in both excitatory and inhibitory cells. A,** Single-cell mutual information, I(S,R), of excitatory neurons during locomotion for optogenetic light-off versus light-on (light-off 0.91 ± 0.03 to light-on 0.64 ± 0.03, p=2.9e-9, n=141 cells). Dashed line indicates unity. **B,** Accuracy in LDA-LOOXV classification of visual stimulus movement orientation, as a population (0.98 to 0.81, p=2e-11, Wilcoxon rank-sum test). Error bars indicate bootstrapped estimates of SE. **C,** Classification accuracy for grating movement orientation as a function of population spike count. Error bars indicate bootstrapped estimates of SE. Chance level would be at 0.16. *p<0.05, **p<0.01. **D,** Same as in A for inhibitory neurons (1.09 ± 0.05 to 0.76 ± 0.05, p=2.4e-5, n=58 cells). **E,** Same as in B for inhibitory neurons (0.86 to 0.58, p=1e-13). **F,** Same as in C for inhibitory neurons.

air. Inhibition of SOM nRT cells produced mostly opposite effects. These findings provide evidence for a specific neural circuit that regulates gamma oscillations, which are associated with visual attention, and the encoding of visual information in V1.

Does nRT activity merely turn off the input to V1? Activation of SOM nRT neurons caused a reduction in firing of both excitatory and putative fast spiking inhibitory neurons in V1, presumably due to a reduction in activity in dLGN thalamocortical relay neurons which are targeted by SOM nRT GABAergic inputs. Interestingly, activating SOM nRT neurons did not just change the firing rate in V1, it also reorganized the pattern of the firing. There was less information during activation of SOM nRT neurons even for responses to visual stimuli that evoked the same number of spikes in single neurons.

Two pathways that modulate V1 activity. Locomotion increases both gamma oscillations and visual responses in mouse V1 and gates a form of adult plasticity (Niell and Stryker, 2010; Kaneko and Stryker, 2014; Kaneko et al., 2017; Hoseini et al., 2019). The effects of locomotion are produced by a circuit operating through vasoactive intestinal peptide (VIP) interneurons in V1 (Fu et al., 2014, 2015). The effects of SOM nRT cells on V1 were more or less additive with those of locomotion. During locomotion, when V1 gamma oscillations are strong, activation of SOM cells in the nRT reduced them. Visual responses of both excitatory and inhibitory cortical neurons were reduced to a similar extent by activation of SOM nRT cells. These findings indicate that these two modulatory systems—locomotion and SOM nRT activation—contribute independently to activity in V1.

Bottom-up versus top-down regulation of V1 activity. SOM nRT cells receive inputs from mainly subcortical structures (central amygdala, anterior thalamus, external segment of globus pallidus) in contrast with PV nRT cells which mainly receive sensory cortical inputs (Clemente-Perez et al., 2017). We speculate that the SOM nRT cells are well positioned to exert a bottom-up regulation of visual attention. In contrast, the effects of locomotion on V1 activity are regulated by cortical VIP interneurons, which are ideally positioned, with dendrites in layer 1, to receive top down inputs from higher cortical areas.

Implications of our findings in disease. Sensory stimulation in the gamma range has been shown to enhance cognition in a mouse model of Alzheimer's disease (Adaikkan et al., 2019). Given that nRT is involved in sensory processing and attention, and that its dysfunction has been implicated in attention disorders (Zikopoulos and Barbas, 2012; Wells et al., 2016), we propose that SOM nRT cells could be a target for modulating gamma oscillations in V1 and visual attention.

MATERIALS AND METHODS

Animals

We performed all experiments in compliance with protocols approved by the Institutional Animal Care and Use Committees at the University of California, San Francisco and Gladstone Institutes. Precautions were taken to minimize stress and the number of animals used in all experiments. Adult (P60–P180) male mice were used. SOM-Cre mice (Sst-IRES-Cre, IMSR_JAX: 018973; C57BL/6 x 129S4/Sv-Jae); PV-Cre mice (PV-Cre, IMSR_JAX: 017320; C57BL/6 congenic); C57BL/6J mice (wild-type, IMSR_JAX: 000664) were used.

Viral delivery in nRT for optogenetic experiments

We performed stereotaxic injections of viruses into the nRT as described (Paz et al., 2011, 2013; Clemente-Perez et al., 2017; Ritter-Makinson et al., 2019). We targeted the nRT with the following stereotaxic coordinates: 1.3 mm posterior to bregma and 2.0-2.1 mm lateral to the midline at two different injection depths (200 nl at 2.65 and 200 nl at 3.0 mm) ventral to the cortical surface. We previously validated this protocol to show specific expression of the viral construct in the nRT neurons and not in surrounding brain areas (Clemente-Perez et al., 2017) (see also **Figure 1**). To determine the effects of SOM neuron activation or inhibition on cortical rhythms and behavior, we injected AAV viruses encoding ChR2-eYFP or eNpHR3.0-eYFP in the nRT of SOM-Cre mice as previously described (Clemente-Perez et al., 2017). For control experiments, we injected AAV viruses containing eYFP in SOM-Cre mice or opsin-expressing viruses in wild-type mice. The location of viral expression was validated by histology after euthanasia in mice whose brains we were able to recover and process.

Headplate surgery and implanting fiber optic

Three to six weeks after viral injections in the nRT, we performed a second surgery to implant a fiber optic in nRT at 1.3 mm posterior to bregma, 1.9-2.0 mm lateral to the midline and 2.3-2.5 mm ventral to the cortical surface; and a titanium headplate – circular center with a 5 mm central opening – above the V1 cortex at -2.9 mm posterior to bregma, and 2.5 mm lateral to the midline. The base of the fiber optic and the entire skull, except for the region above V1, was covered with Metabond (Parkell Co.). One week after the recovery from this surgery, the animal was allowed to habituate to the recording setup by spending 15-30 minutes on the floating ball over the course of one to three days, during which time the animal was allowed to run freely. About two weeks following this surgery (i.e. ~4-6 weeks after viral injection in nRT), the animal's head was fixed to a rigid crossbar above a floating ball. The polystyrene ball was constructed using two hollow 200-mm-diameter halves (Graham Sweet Studios) placed on a shallow polystyrene bowl (250 mm in diameter, 25 mm thick) with a single air inlet at the bottom. Two optical USB mice, placed 1 mm away from the edge of the ball, were used to sense rotation of the floating ball and transmit signals to our data analysis system using custom driver software. These measurements are used to divide data into still and running trials and analyze them separately.

Microelectrode recordings in alert mice

To control for circadian rhythms, we housed our animals using a fixed 12 hr reversed light/dark cycle and performed recordings between roughly 11:00 AM and 6:00 PM. All the recordings were made during wakefulness in awake, head-fixed mice that were free to run on the floating ball (**Figure 2A)** (Hoseini et al., 2019). On the day of recording, the animal was anesthetized with isoflurane (3% induction, 1.5% maintenance) and a craniotomy of about 1 mm in diameter was made above V1 (-2.9 mm posterior to bregma, and 2.5 mm lateral from midline). After animals recovered from anesthesia for at least one hour, a 1.1-mm-long double-shank 128-channel electrode (Du et al., 2011), fabricated by the Masmanidis laboratory (University of California, Los Angeles) and assembled by the Litke laboratory (University of California, Santa Cruz), was slowly inserted through the cranial window. The electrode was placed at an angle of 20-40° to the normal of the cortical surface and inserted to a depth of ~1000 μm. An optical fiber (200 μm diameter) coupled to a light source (green laser for eNpHR, peak intensity ~104 mW/mm^2 at 532 nm; blue laser for ChR2, peak intensity ~63 mW/mm^2 at 473 nm) was connected to the implanted fiber optic in order to deliver light into nRT. Laser power (3-20mW)

		Still & laser-off	Still & laser-on	Running & laser-off	Running & laser-on	p-value
Fig. 2C (n=111 channels)	θ	39 ± 1.8	27 ± 1.4			1.2e-9
	β	64 ± 3.4	38 ± 2.3			4.7e-10
	γ	131 ± 6.5	67 ± 4.4			2.5e-12
Fig. 2D (n=111 channels)	θ	39 ± 1.8		45 ± 2.8		0.70
	β	64 ± 3.4		49 ± 2.7		4.5e-5
	γ	131 ± 6.5		201 ± 9.2		5.2e-12
Fig. 2E (n=4 mice)	θ	29 ± 7.1	1.8e4 ± 5.0	33 ± 10.6	32 ± 9.5	0.34 (still), 0.88 (running)
	β	47 ± 10.0	2.7e4 ± 6.3	36 ± 6.0	32 ± 6.4	0.34 (still), 0.68 (running)
	γ	95 ± 18.5	5.0e4 ± 10.3	137 ± 31.04	83 ± 17.7	0.11 (still), 0.02 (running)
Fig. 2H (n=94 channels)	θ	-8.9 ± 0.5		16 ± 1.1		0
	β	18 ± 1.6		5.7 ± 1.1		4.9e-9
	γ	39 ± 1.4		-42 ± 1.6		0
Fig. 2I (n=4 mice)	θ	6.2 ± 8.7	1.1e4 ± 7.7	-0.9 ± 2.8	1.9e4 ± 6.4	0.88 (still), 0.02 (running)
	β	22 ± 11.9	3.3e4 ± 5.9	3.7 ± 2.9	1.5e4 ± 7.4	0.34 (still), 0.20 (running)
	γ	17 ± 7.6	-2.3e4 ± 7.1	19 ± 8.5	-2.8e4 ± 9.2	0.02 (still), 0.02 (running)
Fig. 2K (n=134 BS, 51 NS)	BS	10.6 ± 1.61	6.9 ± 1.00	16.9 ± 2.65	10.5 ± .59	0.13 (still), 0.08 (running)
	NS	15.98 ± 2.94	9.2 ± 1.33	25.9 ± 4.34	15.2 ± 2.40	0.08 (still), 0.02 (running)
Fig. 2L (n=100 BS, 32 NS cells)	BS	-38.2 ± 0.83	-23.6 ± 4.72	-38.2 ± 1.01	-34.0 ± 4.02	
	NS	-38.5 ± 0.65	-21.1 ± 8.10	-38.0 ± 1.17	-35.56 ± 5.31	
Fig. 3B (n=121 channels)	θ	22 ± 1.4	22 ± 1.4			0.78
	β	42 ± 5.3	45 ± 5.5			0.50
	γ	77 ± 12.5	78 ± 12.4			0.88
Fig. 3C (n=121 channels)	θ	22 ± 1.4		27 ± 2.0		0.04
	β	42 ± 5.3		42 ± 4.5		.49
	γ	77 ± 12.5		99 ± 12.2		0.004
Fig. 3E (59 channels)	θ	27 ± 0.3	3.3 ± 0.4			0.45
	β	4.0 ± 0.8	4.7 ± 0.7			1.5e-6
	γ	6.6 ± 1.8	6.5 ± 1.2			0.33
Fig. 3F (n=31 BS, 43 NS cells)	BS	10.8 ± 1.72	11.8 ± 1.81	15.8 ± 2.64	16.1 ± 2.75	0.66 (still), 0.96 (running)
	NS	12.0 ± 2.13	12.3 ± 2.15	18.9 ± 4.05	18.3 ± 3.90	0.85 (still), 0.92 (running)
Fig. 5C (n=102 channels)	θ	54 ± 1.9	49 ± 1.8			9.2e-3
	β	63 ± 2.1	77 ± 2.6			5.2e-5
	γ	90 ± 2.9	146 ± 4.7			0
Fig. 5D (n=102 channels)	θ	54 ± 1.9		49 ± 1.6		0.01
	β	63 ± 2.1		68 ± 2.5		0.48
	γ	90 ± 2.9		197 ± 7.7		0
Fig. 5E (n=4 mice)	θ	45 ± 6.8	44 ± 7.4	56 ± 9.5	43 ± 4.0	1.143 (still), 0.34 (running)
	β	66 ± 13.0	70 ± 15.8	65 ± 11.2	67 ± 14.5	0.88 (still), 0.88 (running)
	γ	94 ± 19.0	119 ± 28.0	130 ± 30.0	169 ± 34.5	0.48 (still), 0.48 (running)
Fig. 5H (n=120 channels)	θ	6.0 ± 0.6		-21 ± 1.3		0
	β	20 ± 1.6		7 ± 0.8		2.4e-10
	γ	16 ± 1.2		74 ± 3.3		0
Fig. 5I (n=4 mice)	θ	8.7 ± 1.4	-0.9 ± 7.0	8.2 ± 3.2	-2 ± 4.2	0.34 (still), 0.11 (running)
	β	22 ± 5.1	18 ± 7.2	13 ± 5.8	4 ± 4.6	0.34 (still), 0.34 (running)
	γ	4.0 ± 3.7	32 ± 13.9	12 ± 3.4	25 ± 10.9	0.05 (still), 0.48 (running)
Fig. 5K (n=58 BS, 44 NS cells)	BS	8.0 ± 1.13	9.8 ± 1.5	11.3 ± 1.5	13.4 ± 1.8	0.002 (still), 3.0e-7 (running)
	NS	20.4 ± 2.3	29.5 ± 3.5	31.6 ± 3.3	41.9 ± 4.1	1.1e-6 (still), 2.1e-8 (running)
Fig. 5L (n=68 BS, 22 NS)	BS	27.8 ± 1.8	21.7 ± 8.3	13.5 ± 1.0	16.9 ± 2.3	
	NS	24.2 ± 4.2	28.0 ± 5.8	13.3 ± 1.6	15.2 ± 2.8	

Table 1. Results of significance testing across different conditions. Power amplitudes are in units of 1,000*μV²/Hz (**Figs**. **2C-I**, **3B-E**, **5C-I**) and firing rates are in Hz (**Figs**. **2K**, **2L**, **3F**, **5K**, **5L**).

was measured at the end of the optical fiber before connecting to the animals. Recordings were started an hour after electrode insertion in V1.

Visual stimuli

Stimuli were displayed on an LCD monitor (Dell, 30x40 cm, 60 Hz refresh rate, 32 cd/m^2 mean luminance) placed 25 cm from the mouse and encompassing azimuths from -10° to 70° in the contralateral visual field and elevations from -20° to +40°. In the first set of recordings, no stimulus was presented (uniform 50% gray) while nRT was exposed to the optogenetic light for 4 s every 20 s. For the second set of recordings, drifting sinusoidal gratings at 8 evenly spaced directions (20 repetitions, 2 s duration, 0.04 cycles per degree, and 1 Hz temporal frequency) were generated and presented in random sequence using the MATLAB Psychophysics Toolbox (Brainard, 1997; Kleiner et al., 2007) followed by 2-second blank period of uniform 50% gray. This stimulus set was randomly interleaved with a similar set in the presence of optogenetic light. Optogenetic stimulation was delivered for 2 s periods beginning simultaneously with the onset of the visual stimulus, overlapping the entire stimulus period and turns off by the end of the stimulus.

Data acquisition

Movement signals from the optical mice were acquired in an event-driven mode at up to 300 Hz, and integrated at 100-ms-long intervals and then converted to the net physical displacement of the top surface of the ball. A threshold was calculated individually for each experiment (1-3 cm/s), depending on the noise levels of the mouse tracker, and if the average speed of each trial fell above the threshold, the mouse was said to be running in that trial. Running speed of the animal was used to divide trials into either a running or still state that were analyzed separately. Data acquisition was performed using an Intan Technologies RHD2000-Series Amplifier Evaluation System, sampled at 20 kHz; recording was triggered by a TTL pulse at the moment visual stimulation began. Spike responses during a 1000 ms period beginning 500 ms after stimulus onset were used for analysis.

Single-neuron analysis

The data acquired using 128-site microelectrodes were sorted using MountainSort (Chung et al., 2017), which allows for fully automated spike sorting and runs at 2x real time. Manual curation after a run on 40 minutes of data takes an additional 20 minutes, typically yielding 90 (range 50 –130) isolated single units. Using average waveforms of isolated single units, three parameters were defined in order to classify single units into narrow- or broad-spiking (Niell and Stryker, 2008). The parameters are as follows: the height of the positive peak relative to the negative trough, the slope of the waveform 0.5 ms after the negative trough, and the time from the negative trough to the peak (see **Figure 3E**).

Mutual information

Neuronal responses are considered informative if they are unexpected. For example, in the context of visually evoked neural activity, if a neuron responds strongly to only a very specific stimulus, e.g. photographs of Jennifer Aniston (Quiroga et al., 2005), the response is informative. In contrast if a neuron consistently produces a similar number of spikes per second to all presented stimuli, this response provides little information. This notion can be formalized by a measure of information called the Shannon entropy,

$$H(X) = E_X[I(x)] = -\sum_{x \epsilon X} p(x)\log_2 p(x)$$

where H(X) is in units of bits. The neuron that responds to Jennifer Aniston's face has high entropy and is therefore said to be informative. The concept is further extended to mutual information, $I(S, R)$, which quantifies how much information the neuronal response (R) carries about the visual stimulus (S) by computing the average reduction in uncertainty (entropy) about the visual stimulus produced by observing neuronal responses. Intuitively, observing responses from the aforementioned Jennifer Aniston neuron leaves little uncertainty as to which face was presented. Mutual information between S and R is calculated as follows:

$$I(S,R) = H(S) - H(S|R) = E_X[I(x)]$$
$$= \sum_{r \in R} \sum_{s \in S} p(r,s) \log_2 (p(r,s) / p(r)p(s))$$

where r and s are particular instances from the set of neural responses (measured as spike counts) and stimuli (grating movement directions), respectively. We used Information Theory Toolbox in MATLAB to compute mutual information (https://www.mathworks.com/matlabcentral/fileexchange/35625-information-theory-toolbox).

Population-based analysis: decoding the visual stimulus from population responses

Data trials were separated into equal numbers of laser-off and -on trials. We then randomly subsampled from each 50 times to get a distribution of decoding errors based on the data included. We trained a linear discriminant analysis (LDA) classifier to classify single-trial neural responses, assuming independence between neurons (a diagonal covariance matrix). We used a leave-one-out approach to train and test classification separately for each condition (LDA-LOOXV). The classifier was trained and tested using MATLAB's fitcdiscr and predict functions. To decode only grating orientation and not movement direction, we grouped stimuli moving 180° apart into the same class.

Population-based analysis: decoding with equal population spike counts

To determine whether optogenetic manipulation of firing rates are the sole determinants of changes in information content of neuronal responses, we compared decoding accuracy from trials in laser-off and laser-on conditions with equal population spike counts, the sum of spikes from all neurons. This was accomplished by selecting subsets of neurons from the population (1-70 neurons were randomly sub-sampled with replacement). The constructed datasets retain higher-order structure between neural activity with the population but have many samples of laser-off and laser-on trials with the same population spike counts. We used an LDA-LOOXV to train and test classification separately for each subset. For each number of neurons, we subsampled with replacement 100 times from the population, yielding 100 combinations of neurons. Classifiers were trained separately on each subsample and for each condition.

Immunostaining, Microscopy, and Image Analysis

Immunohistochemistry on mouse brain sections and image analysis were performed as previously described (Clemente-Perez et al., 2017; Ritter-Makinson et al., 2019). Briefly, serial coronal sections (50 μm thick) were cut on a Leica SM2000R Sliding Microtome. Sections were mounted in an antifade medium (Vectashield) and imaged using either a Biorevo BZ-9000 Keyence microscope or a confocal microscope. The expression of the viral constructs in different brain regions was confirmed with reference to a standard mouse brain atlas (Paxinos and Franklin, 2001).

Experimental design and statistical analysis

The experiments reported here were designed to determine (i) whether specific cell types in nRT project to visual thalamus and (ii) whether optogenetic activation/inhibition of SOM cells in nRT alters visual responses in V1. For the anatomical experiments, we performed immunohistochemistry of brain sections from 2 SOM-Cre (male) and 3 PV-Cre (male) mice (age range 2 to 4 months). For the physiology experiments, we recorded from 4 mice (male) with optogenetic activation and 4 mice (male) with optogenetic inhibition (age range 3 to 5 months). For the control experiment, we recorded 2 mice (male, age P80) which were injected with a viral construct expressing eYFP in nRT. All data are illustrated in Figures 1-6 and Supplementary Figures 1-3. The main sources of variability for all of optogenetic experiments are the individual neurons and recording sites.

All numerical values are given as means ± SEM and error bars are SEM unless stated otherwise in the figure legends. Parametric and non-parametric tests were chosen as appropriate and were reported in Table 1 and figure legends. Data analysis was done in MATLAB (SCR_001622), Origin 9.0 (Microcal Software, SCR_002815), GraphPad Prism 6 (SCR_002798), R-project (SCR_001905), and SigmaPlot (SCR_003210) using Wilcoxon rank-sum, Wilcoxon signed-rank test, Spearman rank-order correlation with the Bonferroni correction for multiple comparisons (*$p < 0.05$, **$p < 0.01$, and ***$p < 0.001$).

AUTHOR CONTRIBUTIONS

Conceptualization, M.S.H., M.P.S., J.T.P.; Opsin injections in nRT, J.T.P., F.S.C., A.C.P., B.H.; Surgical implantation of optical fibers and headplate implants for unit V1 recordings: J.T.P., M.S.H., B.H.; Optogenetic stimulations and recordings *in vivo*: M.S.H.; Supervision of recordings of V1: M.P.S. and J.T.P.; Histology and imaging: A.H.C., I.L., F.S.C.; Data Analysis, M.S.H.; Writing - Original Draft, M.S.H., M.P.S. and J.T.P.; Writing - Review and Editing, M.S.H., M.P.S., and J.T.P.; Funding Acquisition, B.H., M.P.S. and J.T.P.

ACKNOWLEDGEMENTS

J.T.P. is supported by NIH/NINDS grants R00NS078118 and R01NS096369, Gladstone Institutes, the Kavli Institute for Fundamental Neuroscience, Michael Prize, DoD (EP150038), and NSF award #1608236. M.S.H. is supported by NSF award 1822598 and by NIH grant R01EY025174. B.H. is supported by the American Epilepsy Society Postdoctoral Research Fellowship. M.P.S. is supported by NIH grants R01EY002874 and R01EY025174. M.P.S. is a recipient of the Disney Award for Amblyopia Research from Research to Prevent Blindness. A.H.C. is supported by the Berkelhammer award. F.S.C. is supported by NINDS F31 NS111819-01A1, the NSF Graduate Research Fellowship #1144247, and the UCSF Discovery Fellowship. A.C.P. is supported by National Science Foundation Graduate Research Fellowship awards #1650113. This work was also supported by an NIH/NCRR grant (C06 RR018928) to Gladstone Institutes. We thank Meredith Calvert of the Gladstone Histology & Light Microscopy Core for help with confocal microscopy, and Michael Gill and Iris Lo for help with design and analysis of behavioral assays.

REFERENCES

Adaikkan C, Middleton SJ, Marco A, Pao P-C, Mathys H, Kim DN-W, Gao F, Young JZ, Suk H-J, Boyden ES, McHugh TJ, Tsai L-H (2019) Gamma Entrainment Binds Higher-Order Brain Regions and Offers Neuroprotection. Neuron 102:929-943.e8.

Atencio CA, Schreiner CE (2008) Spectrotemporal Processing Differences between Auditory Cortical Fast-Spiking and Regular-Spiking Neurons. J Neurosci 28:3897–3910.

Barthó P, Hirase H, Monconduit L, Zugaro M, Harris KD, Buzsáki G (2004) Characterization of Neocortical Principal Cells and Interneurons by Network Interactions and Extracellular Features. J Neurophysiol 92:600–608.

Brainard DH (1997) The Psychophysics Toolbox. Spat Vis 10:433–436.

Cardin J a, Carlén M, Meletis K, Knoblich U, Zhang F, Deisseroth K, Tsai L-H, Moore CI (2009) Driving fast-spiking cells induces gamma rhythm and controls sensory responses. Nature 459:663–667.

Chung JE, Magland JF, Barnett AH, Tolosa VM, Tooker AC, Lee KY, Shah KG, Felix SH, Frank LM, Greengard LF (2017) A Fully Automated Approach to Spike Sorting. Neuron 95:1381-1394.e6.

Clemente-Perez A, Makinson SR, Higashikubo B, Brovarney S, Cho FS, Urry A, Holden SS, Wimer M, Dávid C, Fenno LE, Acsády L, Deisseroth K, Paz JT (2017) Distinct Thalamic Reticular Cell Types Differentially Modulate Normal and Pathological Cortical Rhythms. Cell Rep 19:2130–2142.

Crabtree JW (2018) Functional Diversity of Thalamic Reticular Subnetworks. Front Syst Neurosci 12.

Crick F (1984) Function of the thalamic reticular complex: The searchlight hypothesis. Proc Natl Acad Sci U S A 81:4586–4590.

Dadarlat MC, Stryker MP (2017) Locomotion Enhances Neural Encoding of Visual Stimuli in Mouse V1. J Neurosci 37:3764–3775.

Doesburg SM, Roggeveen AB, Kitajo K, Ward LM (2008) Large-Scale Gamma-Band Phase Synchronization and Selective Attention. Cereb Cortex 18:386–396.

Du J, Blanche TJ, Harrison RR, Lester HA, Masmanidis SC (2011) Multiplexed, high density electrophysiology with nanofabricated neural probes. PLoS One 6.

Engel AK, Fries P, Singer W (2001) Dynamic predictions: Oscillations and synchrony in top–down processing. Nat Rev Neurosci 2:704–716.

Fu Y, Kaneko M, Tang Y, Alvarez-Buylla A, Stryker MP (2015) A cortical disinhibitory circuit for enhancing adult plasticity. Elife 4:1–12.

Fu Y, Tucciarone JM, Espinosa S, Sheng N, Darcy DP, Nicoll RA, Huang ZJ, Stryker MP (2014) A Cortical Circuit for Gain Control by Behavioral State. Cell 156:1139–1152.

Gentet LJ, Ulrich D (2003) Strong, reliable and precise synaptic connections between thalamic relay cells and neurones of the nucleus reticularis in juvenile rats. J Physiol 546:801–811.

Gray CM, Engel AK, König P, Singer W (1992) Synchronization of oscillatory neuronal responses in cat striate cortex: Temporal properties. Vis Neurosci 8:337–347.

Halassa MM, Acsády L (2016) Thalamic Inhibition: Diverse Sources, Diverse Scales. Trends Neurosci 39:680–693.

Hoseini MS, Rakela B, Flores-Ramirez Q, Hasenstaub AR,

Alvarez-Buylla A, Stryker MP (2019) Transplanted Cells Are Essential for the Induction But Not the Expression of Cortical Plasticity. J Neurosci 39:7529–7538.

Houser CR, Vaughn JE, Barber RP, Roberts E (1980) GABA neurons are the major cell type of the nucleus reticularis thalami. Brain Res 200:341–354.

Kaneko M, Fu Y, Stryker MP (2017) Locomotion Induces Stimulus-Specific Response Enhancement in Adult Visual Cortex. J Neurosci 37:3532–3543.

Kaneko M, Stryker MP (2014) Sensory experience during locomotion promotes recovery of function in adult visual cortex. Elife 2014:1–16.

Kleiner M, Brainard DH, Pelli DG (2007) What's new in Psychtoobox-3? Perception 36:14.

Kreiter A, Singer W (1996) Stimulus-dependent synchronization of neuronal responses in the visual cortex of the awake macaque monkey. J Neurosci 16:2381–2396.

Lam Y-W, Sherman SM (2011) Functional Organization of the Thalamic Input to the Thalamic Reticular Nucleus. J Neurosci 31:6791–6799.

Lien AD, Scanziani M (2013) Tuned thalamic excitation is amplified by visual cortical circuits. Nat Neurosci 16:1315–1323.

McAlonan K, Cavanaugh J, Wurtz RH (2008) Guarding the gateway to cortex with attention in visual thalamus. Nature 456:391–394.

McCormick DA, Bal T (1997) SLEEP AND AROUSAL: Thalamocortical Mechanisms. Annu Rev Neurosci 20:185–215.

Moore AK, Weible AP, Balmer TS, Trussell LO, Wehr M (2018) Rapid Rebalancing of Excitation and Inhibition by Cortical Circuitry. Neuron 97:1341-1355.e6.

Niell CM, Stryker MP (2008) Highly Selective Receptive Fields in Mouse Visual Cortex. J Neurosci 28:7520–7536.

Niell CM, Stryker MP (2010) Modulation of Visual Responses by Behavioral State in Mouse Visual Cortex. Neuron 65:472–479.

Pavlova M, Birbaumer N, Sokolov A (2006) Attentional Modulation of Cortical Neuromagnetic Gamma Response to Biological Movement. Cereb Cortex 16:321–327.

Paxinos G, Franklin KBJ (2001) Paxinos and Franklin's the Mouse Brain in Stereotaxic Coordinates.

Paz JT, Bryant AS, Peng K, Fenno L, Yizhar O, Frankel WN, Deisseroth K, Huguenard JR (2011) A new mode of corticothalamic transmission revealed in the Gria4−/− model of absence epilepsy. Nat Neurosci 14:1167–1173.

Paz JT, Davidson TJ, Frechette ES, Delord B, Parada I, Peng K, Deisseroth K, Huguenard JR (2013) Closed-loop optogenetic control of thalamus as a tool for interrupting seizures after cortical injury. Nat Neurosci 16:64–70.

Phillips EA, Hasenstaub AR (2016) Asymmetric effects of activating and inactivating cortical interneurons. Elife 5:e18383.

Quiroga RQ, Reddy L, Kreiman G, Koch C, Fried I (2005) Invariant visual representation by single neurons in the human brain. Nature 435:1102–1107.

Ray S, Crone NE, Niebur E, Franaszczuk PJ, Hsiao SS (2008a) Neural Correlates of High-Gamma Oscillations (60-200 Hz) in Macaque Local Field Potentials and Their Potential Implications in Electrocorticography. J Neurosci 28:11526–11536.

Ray S, Niebur E, Hsiao SS, Sinai A, Crone NE (2008b) High-frequency gamma activity (80–150Hz) is increased in human cortex during selective attention. Clin Neurophysiol 119:116–133.

Ritter-Makinson S, Clemente-Perez A, Higashikubo B, Cho FS, Holden SS, Bennett E, Chkhaidze A, Eelkman Rooda OHJ, Cornet M-C, Hoebeek FE, Yamakawa K, Cilio MR, Delord B, Paz JT (2019) Augmented Reticular Thalamic Bursting and Seizures in Scn1a-Dravet Syndrome. Cell Rep 26:54-64.e6.

Saleem AB, Lien AD, Krumin M, Haider B, Rosón MR, Ayaz A, Reinhold K, Busse L, Carandini M, Harris KD, Carandini M (2017) Subcortical Source and Modulation of the Narrowband Gamma Oscillation in Mouse Visual Cortex. Neuron 93:315–322.

Sherman SM, Koch C (1986) The control of retinogeniculate transmission in the mammalian lateral geniculate nucleus. Exp Brain Res 63:1–20.

Siegel M, Donner TH, Oostenveld R, Fries P, Engel AK (2008) Neuronal Synchronization along the Dorsal Visual Pathway Reflects the Focus of Spatial Attention. Neuron 60:709–719.

Singer W, Gray CM (1995) Visual feature integration and the temporal correlation hypothesis. Annu Rev Neurosci 18:555–586.

Sohal VS, Zhang F, Yizhar O, Deisseroth K (2009) Parvalbumin neurons and gamma rhythms enhance cortical circuit performance. Nature 459:698–702.

Stryker MP (1989) Is grandmother an oscillation? Nature 338:297–298.

Taylor K, Mandon S, Freiwald WA, Kreiter AK (2005) Coherent Oscillatory Activity in Monkey Area V4 Predicts Successful Allocation of Attention. Cereb Cortex 15:1424–1437.

Wells MF, Wimmer RD, Schmitt LI, Feng G, Halassa MM (2016) Thalamic reticular impairment underlies attention deficit in Ptchd1Y/− mice. Nature 532:58–63.

Yazdan-Shahmorad A, Kipke DR, Lehmkuhle MJ (2013) High gamma power in ECoG reflects cortical electrical stimulation effects on unit activity in layers V/VI. J Neural Eng 10:066002.

Zikopoulos B, Barbas H (2012) Pathways for Emotions and Attention Converge on the Thalamic Reticular Nucleus in

SUPPLEMENTARY FIGURES

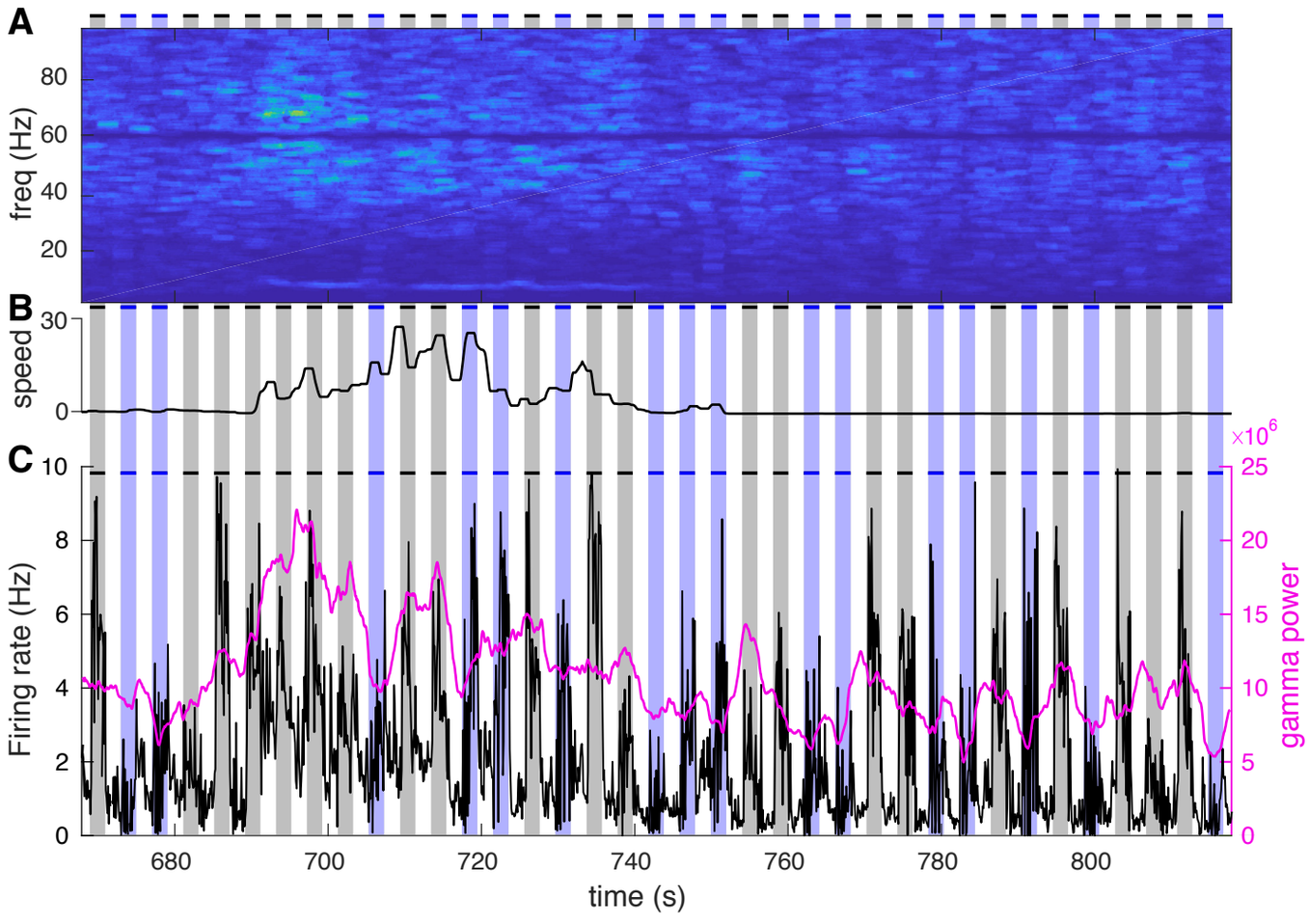

Figure supplement 1. Optogenetic activation of SOM nRT neurons reduces gamma activity in the V1 cortex during visual tasks. A, Representative power spectrum during 150 s of visual exposure only (gray shadings) and visual exposure coupled with optogenetic activation of nRT neurons (blue shadings). **B,** Mouse movement speed. **C,** Average firing rate of all cells (black curve) is shown along with the gamma power (magenta curve). Visual stimuli consistently increase both power and average firing rate while visual exposure coupled with optogenetic activation causes a marked reduction in both measures.

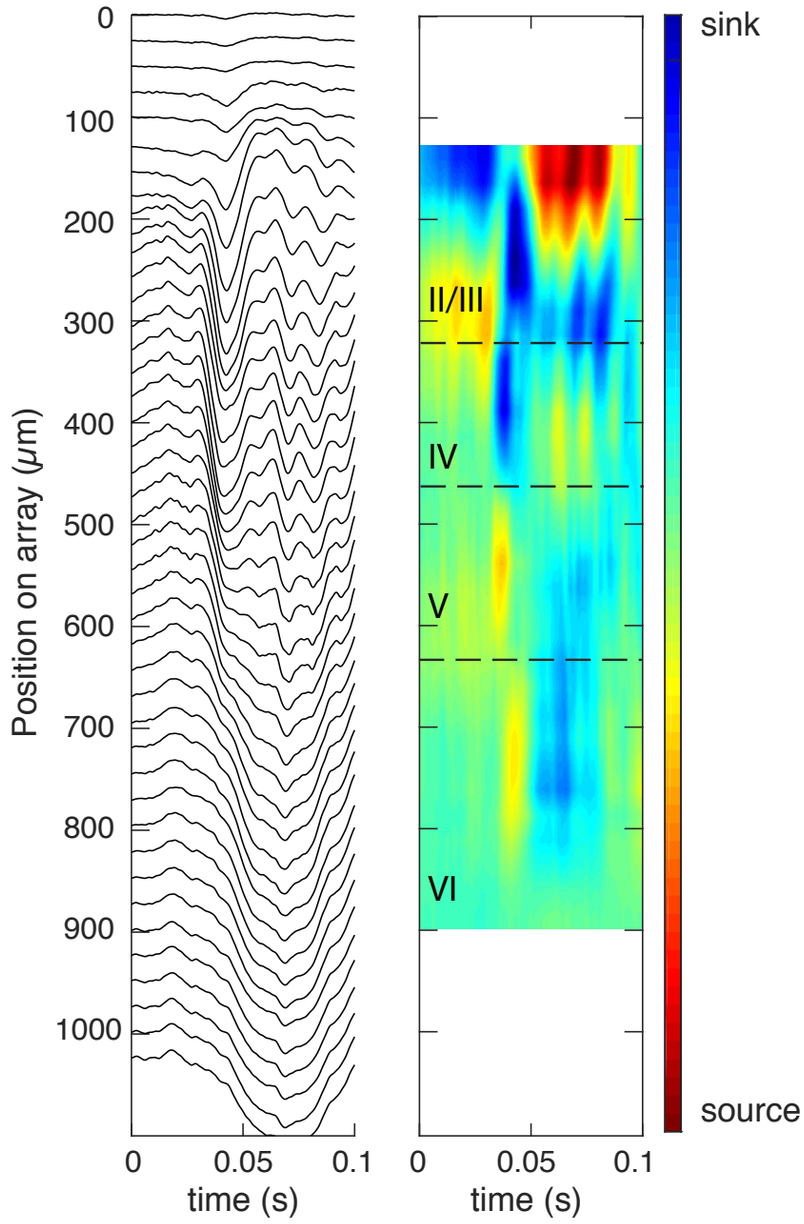

Figure supplement 2. Current source density identifies laminar structure in V1. Local field potential traces averaged over 150 repetition of a contrast-reversing square checkerboard stimulus (left) and current-source density plot for one mouse show laminar structure (right). Distances at left refer to electrode location relative to the top-most recording site of the array.

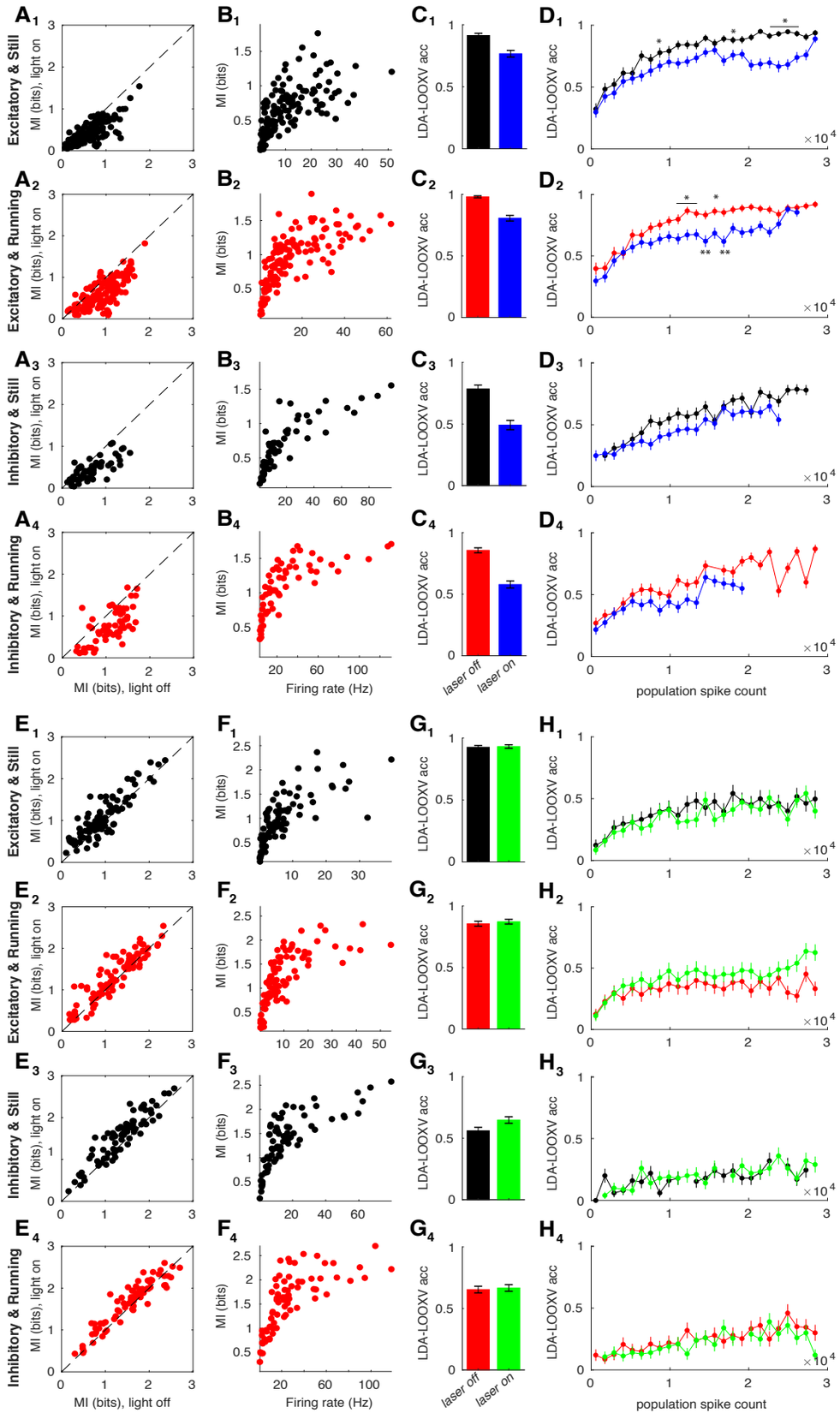
A1
B1
C1
D1
A2
B2
C2
D2
A3
B3
C3
D3
A4
B4
C4
D4
E1
F1
G1
H1
E2
F2
G2
H2
E3
F3
G3
H3
E4
F4
G4
H4
Excitatory & Still
Excitatory & Running
Inhibitory & Still
Inhibitory & Running
MI (bits), light on
MI (bits), light off
MI (bits)
Firing rate (Hz)
LDA-LOOXV acc
laser off
laser on
population spike count
×10^4

Figure supplement 3. Optogenetic manipulation of SOM nRT neurons alters encoding accuracy in both excitatory and inhibitory cells. A, Single-cell mutual information of excitatory neurons while stationary (A_1) and running (A_2), and inhibitory neurons while stationary (A_3) and running (A_4) for optogenetic light-off versus light-on conditions (light-off to light-on; A_1, 0.64 ± 0.03 to 0.42 ± 0.02, p=1e-8, n=141 cells, Wilcoxon signed-rank test; A_2, 0.91 ± 0.03 to 0.64 ± 0.03, p=3e-9; A_3, 0.69 ± 0.05 to 0.45 ± 0.03, p=3e-4, n=58; A_4, 1.09 ± 0.05 to 0.76 ± 0.05, p=2e-5). Dashed line indicates unity. **B,** Single-cell mutual information against firing rate of excitatory neurons while stationary (B_1) and running (B_2), and inhibitory neurons while stationary (B_3) and running (B_4) for light-off (rho, p, Spearman correlation; B_1, 0.76, 7e-28; B_2, 0.84, 4e-38; B_3, 0.9, 0.0; B_4, 0.86, 6e-18). **C,** Accuracy in LDA-LOOXV classification of visual stimulus movement orientation in excitatory neurons during stationary (C_1) and running (C_2), and inhibitory neurons while stationary (C_3) and running (C_4) for light-off versus light-on (light-off to light-on; C_1, 0.91 to 0.77, p=6e-6, Wilcoxon rank-sum test; C_2, 0.98 to 0.81, p=2e-11; C_3, 0.79 to 0.49, p=9e-9; C_4, 0.86 to 0.58, p=1e-13). Error bars indicate bootstrapped estimates of SE. **D,** Classification accuracy for grating orientation as a function of population spike count for excitatory neurons during stationary (D_1) and running (D_2), and inhibitory neurons during stationary (D_3) and running (D_4) for light-off versus light-on. Error bars indicate bootstrapped estimates of SE. Chance level would be at 0.16. *p<0.05, **p<0.01. **E,** Same as in A for optogenetic inhibition of SOM cells in nRT (light-off to light-on; E_1, 0.96 ± 0.05 to 1.10 ± 0.05, p=8e-7, n=90 cells; E_2, 1.19 ± 0.06 to 1.31 ± 0.06, p=1e-4; E_3, 1.35 ± 0.06 to 1.54 ± 0.07, p=9e-9, n=58; E_4, 1.54 ± 0.07 to 1.65 ± 0.07, p=2e-5). **F,** Same as in B during optogenetic inhibition (rho, p, Spearman correlation; F_1, 0.84, 1e-24; F_2, 0.84, 6e-25; F_3, 0.81, 0.0; F_4, 0.82, 2e-19). **G,** Same as in C during optogenetic inhibition (light-off to light-on; G_1, 0.93 to 0.93, p=0.75; G_2, 0.86 to 0.87, p=0.53; G_3, 0.56 to 0.65, p=0.03; G_4, 0.65 to 0.67, p=0.71). **H**, Same as in D during optogenetic inhibition.